SLAC–PUB–5519
April, 1991
(T/E)

Radiative Corrections to $BR(Z \rightarrow b\bar{b})$ in the Minimal Supersymmetric Standard Model*

MICHAEL BOULWARE† AND DONALD FINNELL†

Stanford Linear Accelerator Center

Stanford University, Stanford, California 94309

ABSTRACT

We examine 1-loop vertex corrections to the process $Z \rightarrow b\bar{b}$ in the minimal supersymmetric standard model. The amplitude for this process may be enhanced by large Yukawa couplings which arise in the case of a heavy top or a very large value of $\tan\beta$. This leads to the possibility that SUSY might be observed indirectly by precision measurements of $BR(Z \rightarrow b\bar{b})$.

Submitted to *Physical Review* **D**

* Work supported by the Department of Energy, contract DE–AC03–76SF00515.
† Work supported in part by an NSF Graduate Fellowship.

1. Introduction

A precise measurement of the decay rate for $Z \to b\bar{b}$ has a number of advantages as an indirect test for physics beyond the standard model. It is well known that a heavy top quark gives large contributions to the Z partial widths through its appearance in vacuum polarization diagrams. These corrections grow as m_t^2, but, since they appear only as an overall rescaling of the partial widths and a renormalization of $\sin^2\theta_W$, these effects are essentially universal among fermion species. However, the decay to bottom quarks receives an additional, unique correction, also proportional to m_t^2, arising from the direct coupling of the b to the top quark in vertex and external leg diagrams. This correction has been calculated by a number of authors,[1-3] who find that it results in a 1% reduction in the $Z \to b\bar{b}$ partial width for $m_t = 150$ GeV, increasing to a 3% reduction as m_t goes to 250 GeV. Measurement of the effect is thus difficult but feasible. Once the top quark mass is known, this effect could be used as an indirect test between the minimal standard model and other models which include new direct couplings to the bottom quark. One interesting model of this sort is the minimal supersymmetric extension of the standard model. In a recent paper, Djouadi et al.[4] gave a survey of the effects of a variety of models of new physics on the $Z \to b\bar{b}$ partial width. In this paper, we will reexamine the effects of supersymmetry in somewhat more detail.

Since we are interested in the vertex correction, we would like to consider a measurement which is insensitive to corrections entering indirectly via loops in the Z propagator. An ideal quantity would be the ratio $\Gamma(Z \to b\bar{b})/\Gamma(Z \to s\bar{s})$; clearly all indirect, or oblique, corrections would be the same for both the b and the s, and would cancel in this ratio. Unfortunately this is not measurable in practice, and instead one must look at the ratio $\Gamma(Z \to b\bar{b})/\Gamma(Z \to \text{hadrons})$, henceforth

called R_b. This quantity has only a weak dependence on oblique corrections. To see this, following Boudjema, Djouadi, and Verzegnassi,[5] let us write the $Z \to b\bar{b}$ partial width as

$$\Gamma(Z \to b\bar{b}) = \Gamma_b^{(0)}(1 + \nabla_b^{(t)}(m_t) + 1.49\Delta\rho^{(t)}), \tag{1.1}$$

where $\Gamma_b^{(0)}$ is calculated in the standard model using a small value of the top mass, say $m_t = 50$ GeV. $\nabla_b^{(t)}(m_t)$ contains the m_t dependent parts of the vertex diagrams and behaves as:

$$\nabla_b^{(t)}(m_t) \simeq -\frac{20\alpha}{13\pi}\left(\frac{m_t^2}{M_Z^2}\right) \tag{1.2}$$

for large m_t, while $\Delta\rho^{(t)}$ contains the oblique corrections from a large top mass and has the behavior:

$$\Delta\rho^{(t)} \simeq \frac{\alpha}{\pi}\frac{m_t^2}{M_Z^2}. \tag{1.3}$$

It can then be shown that the branching ratio is given by:

$$R_b = \frac{\Gamma(Z \to b\bar{b})}{\Gamma(Z \to \text{hadrons})} = 0.2196\big(1 + 0.78\nabla_b^{(t)}(m_t) - 0.06\Delta\rho^{(t)}\big). \tag{1.4}$$

We see that that for $m_t = 250$ GeV the oblique term only gives a 0.1% correction, which is negligible when we consider measurements at the 1% level of accuracy. When we add supersymmetry, we will obtain new vertex contributions $\nabla_b^{SUSY}(m_t)$, new oblique corrections $\Delta\rho^{SUSY}$, and the supersymmetric corrections to the branching ratio will be:

$$\begin{aligned}\Delta^{SUSY}(R_b) =& 0.2196\big[0.78(\nabla_b^{SUSY}(m_t) - \nabla_b^{SUSY}(0)) \\ &+ 0.34(\nabla_d^{SUSY}(0) - \nabla_u^{SUSY}(0)) - 0.06\Delta\rho^{SUSY}\big]\end{aligned} \tag{1.5}$$

where $\nabla_{u,d}^{SUSY}(0)$ are the vertex contributions for up and down type quarks, $u, d \neq t, b$. The oblique correction is, again, highly suppresed. $\nabla_d^{SUSY}(0) - \nabla_u^{SUSY}(0)$

is also a negligible quantity, so the supersymmetric contribution to the branching ratio is determined simply by the m_t dependent part of the vertex function, $\nabla_b^{SUSY}(m_t) - \nabla_b^{SUSY}(0)$, which will henceforth be denoted by ∇_b^{SUSY}.

The fact that we need only consider the m_t dependent parts of vertex diagrams greatly simplifies our task. In the minimal supersymmetric model the top mass appears in only a limited number of new couplings, and the number of new diagrams we must evaluate is small. In particular, diagrams involving neutral particles in their loops need not be considered. A possible exception to this rule, the case of large $\tan\beta$, will be discussed in Section 4.

This paper is organized as follows. We briefly review the standard model calculation, and the relevent details of the minimal supersymmetric extension. We then present results for diagrams containing chargino and charged Higgs loops. Finally, we look at the high $\tan\beta$ case and diagrams involving neutralinos and neutral Higgs scalars.

2. The Calculation

In the standard model, the diagrams for the vertex correction to $Z \rightarrow b\bar{b}$ involving top quarks and charged bosons are shown in Figure 1. Several features are worth noting. Since these diagrams involve the exchange of W's, and since the b mass is negligible at the scale we are considering, only the production of left handed b's will be affected. However, this does not result in any significant change in the weak asymmetries, since the tree level amplitude overwhelmingly favored left handed b's to begin with.[6] It is also worth noting that even though the top mass appears in the denominators of top propagators, these diagrams grow with

m_t. This is most easily seen in the 't Hooft-Feynman gauge, where m_t appears in the Yukawa coupling of the b to a charged unphysical Goldstone boson.[1]

Before discussing the additional corrections let us briefly review the relevent features of the minimal supersymmetric model. It is well known that, in supersymmetric models, one cannot give mass to both the top and bottom quarks with a single Higgs doublet. In the minimal case, two seperate Higgs doublets are required. This has two consequences for our calculation. First, in addition to the unphysical Goldstone boson which arises in the standard model, there is a physical charged Higgs boson which will enter our diagrams in loops with the top quark. If H_1 and H_2 are the Higgs doublets giving mass to the top and bottom quarks respectively, the physical charged Higgs is given by:

$$H^+ = \cos\beta H_1^+ + \sin\beta H_2^+, \tag{2.1}$$

where β characterizes the relative sizes of the two vacuum expectation values, $\tan\beta = v_1/v_2$. The charged Goldstone boson is the state orthogonal to this. The minimal model predicts that H^+ will have a mass M_{H^+} which is greater than M_W.[7] The second consequence of the two doublet structure is that relationships between the Yukawa couplings and the quark masses are modified. Whereas in the standard model the top and bottom Yukawa couplings were give by:

$$\lambda_t^{SM} = \frac{g m_t}{\sqrt{2} M_W}, \quad \lambda_b^{SM} = \frac{g m_b}{\sqrt{2} M_W}, \tag{2.2}$$

with the addition of a second doublet these become:

$$\lambda_t = \frac{g m_t}{\sqrt{2} M_W \sin\beta}, \quad \lambda_b = \frac{g m_b}{\sqrt{2} M_W \cos\beta}. \tag{2.3}$$

It follows that H^+ has a coupling to a left handed b proportional to $m_t \cot\beta$ and to a right handed b proportional to $m_b \tan\beta$. We note that values of β for which

$\tan\beta \gg 1$ will lead to a greatly enhanced λ_b. This situation is analyzed in Section 4. For now we assume $\tan\beta$ is of order one and the bottom coupling can be neglected.

The diagrams involving the charged Higgs scalar appear in Figure 2. All diagrams are proportional to $m_t^2 \cot^2\beta$ and their sum is finite. As was the case for the standard model, only left handed b's are affected. We give explicit formulae in Appendix B. These diagrams have been studied in some detail by Hollik[8] in the context of the general two doublet model, and our results are in agreement.

Finally we consider the effects of the supersymmetric particles themselves. Supersymmetry requires that whenever we have a cubic coupling involving 2 fermions and a scalar, $\phi_a\Psi_b\Psi_c + h.c$, it must be part of a larger term $\phi_a\Psi_b\Psi_c + \phi_c\Psi_a\Psi_b + \phi_b\Psi_c\Psi_a + h.c.$, where Ψ_a and ϕ_a are supersymmetric partners. Thus the coupling between the Higgs, right handed top quark and left handed bottom, proportional to λ_t, will be accompanied by a coupling of the same strength between the bottom, higgsino and "right" stop. A more detailed description is given in Appendix A. The only complication is that a mixing term arises between the gauginos and higgsinos, and we must take as mass eigenstates charginos, designated $\chi^{\pm}$, which are mixtures of higgsinos and winos.

Figure 3 shows the supersymmetric diagrams contributing to $\Gamma(Z \to b\bar{b})$. Note that all these diagrams are proportional to $m_t^2/\sin^2\beta$, and have a finite sum. Our explicit result for the supersymmetric contribution is given in Appendix B. For the special case of unmixed squarks, this agrees with the result of Djouadi et al.,[4] except that we find the opposite overall sign. We defend our choice of sign in Appendix B.

In addition to $\tan\beta$ and M_{H+}, there are a number of other parameters in

the supersymmetric lagrangian which enter into this calculation. A coupling μ between the two Higgs fields and a supersymmetry breaking wino mass parameter M enter via the chargino mass matrix. There are also squark mass terms, including in general mixing between the left and right squarks. This is a large number of free parameters, and we shall explore which regions of parameter space yield a significant effect.

3. Results

Now let us consider the size of the effects. Figure 4 is a plot of R_b versus top mass, for sample values of parameters which are chosen to show a maximal effect. Results are shown for the minimal standard model (MSM), the two-doublet model, and the minimal supersymmetric standard model (MSSM).

We see from Fig. 4 that in the standard model the branching ratio is decreased from the tree level expectation. Adding a second Higgs enhances the effect. However adding the supersymmetric particles increases the width $\Gamma(Z \to b\bar{b})$, canceling out to some degree the contribution of the H^+ and the MSM radiative corrections. The fact that supersymmetric contribution is positive unfortunately makes the detection of such effects more difficult. However, the fact that this sign is unique to the supersymmetric contribution would, if observed, provide a clear distinction between this and a non-supersymmetric two-doublet model. We note that for different parameter values, the MSSM result could be anywhere between the two-doublet and MSSM curves of Fig. 4, and for some parameters the H^+ and chargino contributions could cancel, leaving the MSM prediction unchanged.

Numerical results for the H^+ diagrams can be found in Hollik's paper on the two doublet model.[8] For reference we include a plot of $\nabla_b^{(H^+)}$ as a function of M_{H^+}

(Figure 5). We note that while it can be quite large for $\tan\beta = 1$, it falls off as $\tan^{-2}\beta$ and is negligible for $\tan\beta > 2$.

Now let us examine the dependence of supersymmetric diagrams on parameter space. This is difficult to plot as the number of parameters is large. The dependence on m_t however, coming only from Yukawa couplings, is simply quadratic, so we shall take $m_t = 150$ GeV. For different values of m_t our results simply scale as $(m_t/150)^2$. The effects of $\tan\beta$, M, and μ are more subtle as they become mixed up both in the masses of the charginos and in the mixing angles defining the chargino couplings. Perhaps most useful are plots describing the effects of these 3 variables. Raising $\tilde{m}_t$ lowers the magnitude of the effect but changes the dependences on the other parameters very little. For the moment we assume there is no mixing between right and left squarks.

In Figures 6 and 7 we plot contours for $\nabla_b^{(\chi^+)}$ as a function of M and μ, for $\tan\beta = 1$ and $\tan\beta = 10$ respectively. For reference, we have also plotted the limits in parameter space coming from past and future direct searches for supersymmetry. The fact that supersymmetric particles have not been observed in Z decay allows us to exclude regions in the M, μ plane which give chargino masses below 45 GeV. This is shown by the first set of dashed lines. Neutralino masses depend on another supersymmetry breaking parameter, the $U(1)$ gaugino mass M', as well as M and μ. If we assume our model is embedded in a grand unified theory, we may relate M' to M,[9] and then put a stronger limit by asserting that the 2 lightest neutralinos must have a total mass greater than 90 GeV. This is shown by the dotted lines. The second set of dashed and dotted lines show what these same limits will be if supersymmetric particles are not observed directly at LEP2, assuming a center of mass energy of 180 GeV.

From Fig. 6, taking into account the factor of 0.78 appearing in (1.5), we see the maximal chargino contribution to R_b is about 1.2% for $m_t = 150$ GeV. This is a significant effect, slightly larger than the standard model correction. However, this large contribution occurs for values of M and μ along the edge of the region allowed by current chargino mass limits. For these parameters, charginos would soon be directly observable. Perhaps it is more useful to consider how large the effect could be in regions of parameter space which will not be accesible to LEP2. From Fig. 6 we see that the maximum contribution above the second set of limits would be approximately 0.6%. This could still be significant, especially for a top mass somewhat higher than 150 GeV, however we must not forget that it will be partially canceled by the H^+ contribution. In fact, from Fig. 5 we see that a 0.6% chargino contribution would be almost completely canceled for $M_{H^+} \simeq 100$ GeV.

For $\tan\beta = 10$, we see from Fig. 7 that the maximum chargino contribution to R_b would be 0.5%. This is somewhat smaller than the $\tan\beta = 1$ case, mostly because of the $\sin^{-1}\beta$ dependence of top Yukawa coupling. In the region inaccesible to LEP2, the maximum is 0.3%, which is unmeasurably small. For a 250 GeV top quark, however, this grows to a 0.7% effect, none of which will be cancelled since the H^+ contribution is negligible for large $\tan\beta$. These results change very little with $\tan\beta$ for $\tan\beta > 3$.

Finally, let us consider the effect of squark masses and mixings on these results. The above results all assumed that there was no mixing between $\tilde{t}_R$ and $\tilde{t}_L$, and that $\tilde{t}_R$, which couples to the left handed b, has a mass of 100 GeV. In Figure 8 we show the dependence of the chargino graphs on the mass of the right handed squark, for sample values of M, μ. The chargino contribution falls off rapidly with the squark mass, decreasing by 33% as $\tilde{m}_t$ is increased to 150 GeV, and by 50%

when it is increased to 200 GeV. In the case of mixed L and R squarks, we will have mass eigenstates

$$\begin{aligned} \tilde{t}_1 &= \cos\theta \tilde{t}_R + \sin\theta \tilde{t}_L \\ \tilde{t}_2 &= -\sin\theta \tilde{t}_R + \cos\theta \tilde{t}_L. \end{aligned} \tag{3.1}$$

In Figure 9 we assume $\tilde{t}_1$ to have a mass of 100 GeV, and show the dependence of $\nabla_b^{(x^+)}$ on $\tilde{m}_2$ and θ as $\tilde{m}_2$ is varied from 100 to 300 GeV. Obviously, mixing is irrelevent when the two masses are degenerate or nearly so. When there is a large mass difference, the maximum effect occurs when θ is close to zero (actually $\simeq 10^o$), so the effect of mixing is in general to decrease the size of the contribution from the unmixed case.

4. Large Tanβ

In the case where $\tan\beta \gg 1$, a number of interesting new effects arise. The bottom Yukawa coupling constant $\lambda_b \propto m_b/\cos\beta \simeq m_b \tan\beta$ becomes large, and indeed surpasses λ_t at $\tan\beta = m_t/m_b$, and so we may in principle get sizeable contributions from graphs proportional to the bottom coupling, which we ignored before. These include loops with neutral gauginos/higgsinos and neutral Higgs scalars. Also, whereas for low $\tan\beta$ all radiative corrections were to the production of left handed b's, for high $\tan\beta$ the production of right handed b's can be enhanced, and may have an observable effect on the weak asymmetries. We will present corrections to the bottom left-right asymmetry,

$$A_{LR}^b = \left(\frac{\sigma(Z \to b_L \bar{b}_R) - \sigma(Z \to b_R \bar{b}_L)}{\sigma(Z \to b_L \bar{b}_R) + \sigma(Z \to b_R \bar{b}_L)} \right), \tag{4.1}$$

as well as to R_b. A_{LR}^b can be most easily observed in the polarized forward-

backward asymmetry for $b\bar{b}$ production:

$$A^b_{FB,pol.} = \left(\frac{\sigma(e^-_L \to B_F) - \sigma(e^-_L \to B_B) - \sigma(e^-_R \to B_F) + \sigma(e^-_R \to B_B)}{\sigma(e^-_L \to B_F) + \sigma(e^-_L \to B_B) + \sigma(e^-_R \to B_F) + \sigma(e^-_R \to B_B)}\right) \quad (4.2)$$
$$= \frac{3}{4} A^b_{LR}(1 - 2\chi)$$

where χ is the parameter of $B - \bar{B}$ mixing. We will present results for $\tan\beta = 70$; for different large values of $\tan\beta$ simply scale these results as $\tan^2\beta$.

First, we note that the chargino graphs considered earlier have right-handed components proportional to λ_b. Figure 10 shows their contributions to A^b_{LR} and $\nabla^{(\chi^+)}_b$. We notice that the contribution to $\nabla^{(\chi^+)}_b$ is negative, opposite to that from the chargino's left handed contribution, and of a smaller magnitude, and would therefore decrease the net chargino contribution to R_b. The high $\tan\beta$ contribution to A^b_{LR} would be more significant, being up to .01 in the currently allowed region and .003 in the region outside of LEP2 range.

Secondly, neutralinos, neutral gauginos and higgsinos which mix as described in Appendix A, have both left and right handed couplings to the b proportional to λ_b. The relevent diagrams are shown in Fig. 11. . Figures 12 and 13 show contours for $\nabla^{(\chi^0)}_b$ and for the neutralino contribution to A^b_{LR}. We see that there is a region along the edge of the currently allowed parameter space where the contribution to R_b would be quite large, and in this region it would be positive and enhance the chargino contribution. Unfortunately, the neutralino contribution falls off rapidly away from this region and is negligible outside the LEP2 boundary. Thus it would only have a significant effect in the case where supersymmetric particles would soon be directly observable anyway.

Finally, we must consider contributions from the neutral Higgs scalars, and from the right handed couplings of the charged Higgs scalar considered earlier. In

the minimal supersymmetric model, there is one physical pseudoscalar,

$$A^0 = \cos\beta \mathrm{Im}(H_1^0) + \sin\beta \mathrm{Im}(H_2^0), \tag{4.3}$$

and two neutral scalars,

$$H^0 = \sin\alpha \mathrm{Re}(H_1^0) + \cos\alpha \mathrm{Re}(H_2^0) \tag{4.4}$$

$$h^0 = \cos\alpha \mathrm{Re}(H_1^0) - \sin\alpha \mathrm{Re}(H_2^0). \tag{4.5}$$

H^0 and h^0 have Yukawa couplings to b proportional to $\lambda_b \cos\alpha$ and $\lambda_b \sin\alpha$ respectively, and A^0 has a coupling porportional to $\lambda_b \sin\beta\gamma^5$, so the diagrams in Figure 14 give contributions proportional to $m_b^2 \tan^2\beta$. These diagrams are studied in some detail in a recent paper by Denner et al. on the non-supersymmetric two-doublet model.[10] The MSSM gives tree level relations between the masses of these particles,[7] which are rather simple in the limit of large $\tan\beta$:

$$M_{H^+}^2 = M_W^2 + M_{A^0}^2 \tag{4.6}$$

$$M_{H^0} = \max\{M_Z, M_{A^0}\} \quad M_{h^0} = \min\{M_Z, M_{A^0}\} \tag{4.7}$$

with

$$\alpha = \begin{cases} -\beta \simeq -\frac{\pi}{2}, & M_{A^0} < M_Z; \\ 0, & M_{A^0} > M_Z. \end{cases} \tag{4.8}$$

In Figure 15 we plot $\nabla_b^{(H)}$, which includes the effects both charged and neutral Higgs scalars, and the scalar contribution to A_{LR}^b, as a function of M_{A^0}, using these tree level relations. For a pseudoscalar mass near 45 GeV there would be a

large positive contribution to R_b which would enhance the chargino and neutralino contributions, while for larger M_{A^0} it would be smaller and negative. The scalar contribution to A_{LR}^b would be positive and would add constructively with the chargino contribution.

5. Conclusion

In the minimal supersymmetric standard model, radiative corrections to the ratio $\Gamma(Z \to b\bar{b})/\Gamma(Z \to \text{hadrons})$ could result in an increase in this quantity over the standard model expectation. However, this effect would be detectable at the 1% level of experimental accuracy only in a limited region of supersymmetry parameter space, much of which will be ruled out if supersymmetric particles are not observed directly at LEP2. The usefulness of this process as a complement to direct searches for supersymmetry ultimately depends on the top mass; for $m_t \simeq 150$ GeV its usefulness would be rather limited, while if the top mass were surprisingly large, say $m_t \simeq 250$ GeV, it might still provide a significant opportunity.

The authors thank M. Peskin for suggesting this topic and for many useful conversations.

APPENDIX A

For reference, we give the parts of the supersymmetric lagrangian relevent to this calculation. For a more complete treatment, see for example Gunion and Haber.[11] We borrow much of our notation from Haber and Kane.[9]

The supersymmetric particles entering this calculation are the following: the

gauginos,

$$\tilde{W}^{\pm} = \frac{1}{\sqrt{2}}(\tilde{W}^1 \mp i\tilde{W}^2), \quad \tilde{W}^3, \quad \tilde{B}, \tag{A.1}$$

the higgsinos,

$$\tilde{H}^{(1)} = \begin{pmatrix} \tilde{H}_1^0 \\ \tilde{H}^+ \end{pmatrix} \quad \tilde{H}^{(2)} = \begin{pmatrix} \tilde{H}^- \\ \tilde{H}_2^0 \end{pmatrix} \tag{A.2}$$

and the squarks, $\tilde{t}_L, \tilde{t}_R$ and $\tilde{b}_L, \tilde{b}_R$. Fermions are represented here by two component left-handed Weyl spinors. The Higgs and higgsinos are taken to be members of the conjugate representation of $SU(2)_L$. The squarks are chosen to have the conventional quantum numbers of their spin 1/2 partners.

Let b, t represent the left handed components of quark fields, and $\bar{b}$, $\bar{t}$ the right handed components, all in the left handed Weyl representation. The Higgs-quark couplings and their supersymmetric counterparts are then:

$$\begin{aligned} \mathcal{L}_{qH} = &- \lambda_t\{H_i^{(1)}(\bar{t}Q_i) + \tilde{t}_R^{\dagger}(\tilde{H}_i^{(1)}Q_i) + \tilde{Q}_i(\tilde{H}_i^{(1)}\bar{t})\} \\ &- \lambda_b\{H_i^{(2)}(\bar{b}Q_i) + \tilde{b}_R^{\dagger}(\tilde{H}_i^{(2)}Q_i) + \tilde{Q}_i(\tilde{H}_i^{(2)}\bar{b})\} + \text{h.c.}, \end{aligned} \tag{A.3}$$

where $Q_{1,2} = t, b$. Here, for two spinors ψ and χ, $(\psi\chi) = \epsilon^{\alpha\beta}\psi_\beta\chi_\alpha$.

The higgsinos and winos have the mass term:

$$(-i\tilde{W}^-, \tilde{H}^-)\begin{pmatrix} M & \sqrt{2}M_W \sin\beta \\ \sqrt{2}M_W \cos\beta & \mu \end{pmatrix}\begin{pmatrix} -i\tilde{W}^+ \\ \tilde{H}^+ \end{pmatrix}. \tag{A.4}$$

The mass eigenstates form two Dirac fermions:

$$\chi_i = \begin{pmatrix} \chi_i^+ \\ i\sigma^2(\chi_i^-)^* \end{pmatrix} \quad i = 1, 2 \tag{A.5}$$

$$\chi_i^+ = V_{ij}\psi_j^+ \quad \chi_i^- = U_{ij}\psi_j^- \tag{A.6}$$

where $\psi_{1,2}^{\pm} = -i\tilde{W}^{\pm}, \tilde{H}^{\pm}$. Explicit expresions for V_{ij}, U_{ij}, and the mass eigenvalues

M_i can be found in Ref. 9. The neutralino mass term is:

$$\mathcal{L}_M = -\frac{1}{2}(\psi^0)^T M^0 \psi^0 \tag{A.7}$$

$$M^0 = \begin{pmatrix} M' & 0 & -M_W \sin\beta(\frac{g'}{g}) & M_W \cos\beta(\frac{g'}{g}) \\ 0 & M & M_W \sin\beta & -M_W \cos\beta \\ -M_W \sin\beta(\frac{g'}{g}) & M_W \sin\beta & 0 & -\mu \\ M_W \cos\beta(\frac{g'}{g}) & -M_W \cos\beta & -\mu & 0 \end{pmatrix}$$

$$\psi^0 = \begin{pmatrix} -i\tilde{B} \\ -i\tilde{W}^3 \\ \tilde{H}_1^0 \\ \tilde{H}_2^0 \end{pmatrix} \tag{A.8}$$

The mass eigenstates are the four Majorana fermions:

$$\chi_i^0 = \begin{pmatrix} \chi_i^0 \\ i\sigma^2 \chi_i^{0*} \end{pmatrix} \quad i = 1,4 \tag{A.9}$$

$$\chi_i^0 = N_{ij}\psi_j^0 \tag{A.10}$$

The N_{ij} must be calculated numerically. The squark mass matrix is conventionally parameterized as:

$$(\tilde{t}_L^\dagger, \tilde{t}_R^\dagger) \begin{pmatrix} L^2\tilde{m}^2 + m_t^2 & A\tilde{m}m_t \\ A\tilde{m}m_t & R^2\tilde{m}^2 + m_t^2 \end{pmatrix} \begin{pmatrix} \tilde{t}_L \\ \tilde{t}_R \end{pmatrix} \tag{A.11}$$

The mass eigenstates are $\tilde{t}_i = T_{ij}\tilde{\phi}_j$ where $\tilde{\phi}_{1,2} = \tilde{t}_{L,R}$. An explicit expression for T_{ij} can be found in Ref 9.

In four component notation, the quark fields are

$$b = \begin{pmatrix} b \\ i\sigma^2 \bar{b}^* \end{pmatrix} \quad t = \begin{pmatrix} t \\ i\sigma^2 \bar{t}^* \end{pmatrix} \tag{A.12}$$

The coupling of the charged Higgs scalar to the bottom is:

$$-\left(\frac{g}{\sqrt{2}M_W}\right) H^+ \bar{t}(m_t \cot\beta P_L + m_b \tan\beta P_R) b + \text{h.c.}, \tag{A.13}$$

where $P_L = \frac{1}{2}(1-\gamma^5)$ and $P_R = \frac{1}{2}(1+\gamma^5)$. The couplings of the b quark to supersymmetric particles are:

$$\begin{aligned} \mathcal{L}_{\text{int}} =& g V_{i1}^* \tilde{t}_L^\dagger (\bar{\chi}_i^c P_L b) - \lambda_t V_{i2}^* \tilde{t}_R^\dagger (\bar{\chi}_i^c P_L b) - \lambda_b U_{i2} \tilde{t}_L^\dagger (\bar{\chi}_i^c P_R b) \\ &+ \frac{\sqrt{2}}{3} g' N_{i1} \tilde{b}_R^\dagger (\bar{\chi}_i^0 P_R b) - \lambda_b N_{i4} \tilde{b}_L^\dagger (\bar{\chi}_i^0 P_R b) \\ &+ \frac{1}{\sqrt{2}} \left(\frac{g'}{3} N_{i1}^* - g N_{i2}^*\right) \tilde{b}_L^\dagger (\bar{\chi}_i^0 P_L b) - \lambda_b N_{i4}^* \tilde{b}_R^\dagger (\bar{\chi}_i^0 P_L b) + \text{h.c.} \end{aligned} \tag{A.14}$$

$$\chi_i^c = \begin{pmatrix} \chi_i^- \\ i\sigma^2 (\chi_i^+)^* \end{pmatrix} \tag{A.15}$$

where we have included gaugino couplings as well as higgsino couplings. Feynman rules for the quark-squark-guagino/higgsino vertices follow readily from this expression. This lagrangian uses the convention $\mathcal{D}_\mu = \partial_\mu - ig\vec{T} \cdot \vec{W}_\mu$.

APPENDIX B

We give here explicit formulae for the vertex functions.

In the limit of vanishing bottom mass, the effect of the vertex diagrams can be written as a change in the effective left and right handed couplings between the Z and the b:

$$\begin{aligned} v_L' &= v_L + \frac{\alpha}{4\pi \sin^2\theta_W} F_L(P^2, m_t) \\ v_R' &= v_R + \frac{\alpha}{4\pi \sin^2\theta_W} F_R(P^2, m_t), \end{aligned} \tag{B.1}$$

where

$$v_L = -\frac{1}{2} + \frac{1}{3}\sin^2\theta_W \quad v_R = \frac{1}{3}\sin^2\theta_W. \tag{B.2}$$

The functions $F_{L,R}$ are related to the function ∇_b by:

$$\nabla_b = \frac{\alpha}{4\pi \sin^2\theta_W}\left(\frac{2v_L F_L(M_Z^2, m_t) + 2v_R F_R(M_Z^2, m_t)}{v_L^2 + v_R^2}\right). \tag{B.3}$$

The functions for the Higgs contribution are:

$$\begin{aligned} F_{L,R}^{(1)} &= b_1(M_{H^+}, m_t, m_b^2) v_{L,R} \lambda_{L,R}^2 \\ F_{L,R}^{(2)} &= \Big\{ [\frac{q^2}{\mu_R^2} c_6(M_{H^+}, m_t, m_t) - \frac{1}{2} - c_0(M_{H^+}, m_t, m_t)] v_{R,L}^{(t)} \\ &\quad + \frac{m_t^2}{\mu_R^2} c_2(M_{H^+}, m_t, m_t) v_{L,R}^{(t)} \Big\} \lambda_{L,R}^2 \\ F_{L,R}^{(3)} &= c_0(m_t, M_{H^+}, M_{H^+})(\frac{1}{2} - \sin^2\theta_W)\lambda_{L,R}^2, \end{aligned} \tag{B.4}$$

where

$$v_L^{(t)} = \frac{1}{2} - \frac{2}{3}\sin^2\theta_W \quad v_R^{(t)} = -\frac{2}{3}\sin^2\theta_W, \tag{B.5}$$

$$\lambda_L = \frac{m_t}{\sqrt{2} M_W \tan\beta} \quad \lambda_R = \frac{m_b \tan\beta}{\sqrt{2} M_W}, \tag{B.6}$$

and μ_R is the mass scale which arises in dimensional regularization. Note that m_b

may be taken as zero except in those places where it is enhanced by $1/\cos\beta$.

The chargino contributions are:

$$
\begin{aligned}
F^{(1)}_{L,R} &= \sum_{i=1,2}\sum_{j=1,2} b_1(\tilde{m}_j, M_i, m_b^2) v_{L,R} |\Lambda^{L,R}_{ji}|^2 \\
F^{(2)}_{L,R} &= \sum_{i=1,2}\sum_{j=1,2}\sum_{k=1,2} c_0(M_k, \tilde{m}_i, \tilde{m}_j)(\frac{2}{3}\sin^2\theta_W \delta_{ij} - \frac{1}{2} T^*_{i1} T_{j1}) \Lambda^{L,R}_{ik} \Lambda^{*L,R}_{jk} \\
F^{(3)}_{L,R} &= \sum_{i=1,2}\sum_{j=1,2}\sum_{k=1,2} \{[\frac{q^2}{\mu_R^2} c_6(\tilde{m}_k, M_i, M_j) - \frac{1}{2} - c_0(\tilde{m}_k, M_i, M_j)] O^{R,L}_{ij} \\
&\quad + \frac{M_i M_j}{\mu_R^2} c_2(\tilde{m}_k, M_i, M_j) O^{L,R}_{ij} \} \Lambda^{L,R}_{ki} \Lambda^{*L,R}_{kj}
\end{aligned}
\tag{B.7}
$$

where

$$
\begin{aligned}
\Lambda^L_{ij} &= T_{i1} V^*_{j1} - \left(\frac{m_t}{\sqrt{2} M_W \sin\beta}\right) T_{i2} V^*_{j2} \\
\Lambda^R_{ij} &= -\left(\frac{m_b}{\sqrt{2} M_W \cos\beta}\right) T_{i1} U_{j2},
\end{aligned}
\tag{B.8}
$$

M_i are the chargino masses, O^L_{ij}, O^R_{ij} are defined by

$$
\begin{aligned}
O^L_{ij} &= -\cos^2\theta_W \delta_{ij} + \frac{1}{2} U^*_{i2} U_{j2} \\
O^R_{ij} &= -\cos^2\theta_W \delta_{ij} + \frac{1}{2} V_{i2} V^*_{j2},
\end{aligned}
\tag{B.9}
$$

and T_{ij} is the squark mixing matrix defined in Appendix A. These expressions should be subtracted at $m_t = m_b/\cos\beta = 0$ when used to calculate the branching ratio R_b.

These expressions disagree with those appearing previously in the literature[4] by an overall minus sign. The overall sign can be checked by considering those diagrams involving b self energy corrections. If we increase the b mass until it exceeds the sum of the stop and chargino masses, the b will aquire a width into

these particles, and this width will be related to the imaginary part of the b self energy, $\Pi(\not{q})$, as

$$\Gamma(b \to \tilde{t}\chi^-) = -2\ \mathrm{Im}\Pi(m_b). \tag{B.10}$$

The imaginary part of $\Pi(m_b)$ must therefore be negative in this case, and this provides a check on the overall sign of our expression. Once the sign of the external leg diagrams has been established, the signs of the other diagrams are fixed by the cancelation of divergences.

Finally, we give expressions for the neutralino diagrams:

$$\begin{aligned}
F^{(1)}_{L,R} &= \sum_{i=1,4}\sum_{j=1,2} b_1(\tilde{m}_j, M_i, m_b^2) v_{L,R} |\Lambda^{L,R}_{ji}|^2 \\
F^{(2)}_{L,R} &= \sum_{i=1,2}\sum_{j=1,2}\sum_{k=1,4} c_0(M_k, \tilde{m}_i, \tilde{m}_j)(\frac{1}{2}B^*_{i1}B_{j1} - \frac{1}{3}\sin^2\theta_W \delta_{ij})\Lambda^{L,R}_{ik}\Lambda^{*L,R}_{jk} \\
F^{(3)}_{L,R} &= \sum_{i=1,4}\sum_{j=1,4}\sum_{k=1,2} \{[\frac{q^2}{\mu_R^2}c_6(\tilde{m}_k, M_i, M_j) - \frac{1}{2} - c_0(\tilde{m}_k, M_i, M_j)]O^{R,L}_{ij} \\
&\quad + \frac{M_i M_j}{\mu_R^2} c_2(\tilde{m}_k, M_i, M_j) O^{L,R}_{ij}\} \Lambda^{L,R}_{ki}\Lambda^{*L,R}_{kj}
\end{aligned} \tag{B.11}$$

where

$$\begin{aligned}
\Lambda^L_{ij} &= \frac{1}{\sqrt{2}}(\frac{1}{3}\tan\theta_W N^*_{j1} - N^*_{j2})B_{i1} - \left(\frac{m_b}{\sqrt{2}M_W \cos\beta}\right) N^*_{i4}B_{i2}, \\
\Lambda^R_{ij} &= \frac{\sqrt{2}}{3}\tan\theta_W N_{i1}B_{i2} - \left(\frac{m_b}{\sqrt{2}M_W \cos\beta}\right) N_{i4}B_{i1},
\end{aligned} \tag{B.12}$$

and

$$\begin{aligned}
O^L_{ij} &= \frac{1}{2}(N^*_{i4}N_{j4} - N^*_{i3}N_{j3}) \\
O^R_{ij} &= -O^L_{ji}.
\end{aligned} \tag{B.13}$$

Here $\tilde{m}_i$ are the bottom squark masses and B_{ij} is the bottom squark mixing matrix defined analogously to T_{ij}.

The b's and c's here are reduced Passarino-Veltman functions,[12] defined by

$$[b_0, b_1, b_2, b_3](m_1, m_2, q^2) = \int_0^1 \mathrm{dx}\, \log[-q^2 x(1-x) + x m_1^2 + (1-x) m_2^2 - i\epsilon]/\mu_R^2) \times [1, x, (1-x), x(1-x)] \tag{B.14}$$

$$[c_0, c_1](m_1, m_2, m_3) = \int \mathrm{dxdydz}\delta(x+y+z-1) \log(\Delta/\mu_R^2)[1, z]$$
$$[c_2, c_3, c_4, c_5, c_6, c_7](m_1, m_2, m_3) = \int \mathrm{dxdydz}\delta(x+y+z-1)(\mu_R^2/\Delta) \times [1, z, z^2, z^3, x, xy] \tag{B.15}$$

where

$$\Delta = z m_1^2 + x m_2^2 + y m_3^2 - z(1-z) m_b^2 - xy P^2 - i\epsilon. \tag{B.16}$$

For the reader's convenience we give expressions for the functions used here in terms of the conventional Passarino-Veltman functions[13]:

$$\begin{aligned} b_1(m_1, m_2) =& B_1(m_2, m_1) + \frac{1}{2}(\Delta - \ln \mu_R^2) \\ c_0(m_1, m_2, m_3) =& -2C_{24}(m_2, m_1, m_3) + \frac{1}{2}(\Delta - \ln \mu_R^2) \\ c_2(m_1, m_2, m_3) =& \mu_R^2 C_0(m_2, m_1, m_3) \\ c_6(m_1, m_2, m_3) =& -\mu_R^2 [C_{23} + C_{11}](m_2, m_1, m_3), \end{aligned} \tag{B.17}$$

where $\Delta = 1/(2 - d/2) - \gamma - \ln \pi$ is the divergence which arises in dimensional regularization.

REFERENCES

1. J. Bernabeu, A. Pich, and A. Santamaria, *Phys.Lett.* **B200** (1988), 569.
2. W. Beenaker and W. Hollik, *Z.Phys.* **C40** (1988), 141.
3. A. Akhundov, D. Bardin, T. Riemann, *Nucl.Phys.* **B276** (1986), 1.
4. A. Djouadi, G. Girardi, C. Verzegnassi, W. Hollik and F. Renard, *Nucl.Phys.* **B349** (91), 48.
5. F. Boudjema, A. Djouadi and C. Verzegnassi, *Phys.Lett.* **B238** (1990), 423.
6. A. Djouadi, J. Kühn, P. Zerwas, *Z.Phys.* **C46** (1990), 411.
7. J.F.Gunion, H.E.Haber, G.L.Kane, S.Dawson: The Higgs Hunter's Guide, Addison and Wesley Publ. Comp. 1990.
8. W. Hollik, *Mod.Phys.Lett.* **A5** (1990), 1909.
9. H.Haber and G.Kane, *Phys.Rep.* **117** (1985), 75.
10. A. Denner, R. Guth, W. Hollik and J. Kühn, MPI-PAE-PTH-1-91.
11. J. Gunion and H. Haber, *Nucl.Phys.* **B272** (1986), 1.
12. C. Ahn, B. Lynn, M. Peskin, and S. Selipsky, *Nuc.Phys.* **B309** (1988), 221.
13. G. Passarino and M. Veltman, *Nucl.Phys.* **B160** (1979), 151.

FIGURE CAPTIONS

1) Standard model diagrams contributing to $Z \rightarrow b\bar{b}$ in unitary gauge. In renormalizable gauges these are accompanied by diagrams with unphysical charged Goldstone bosons.

2) Charged Higgs diagrams contributing to $Z \rightarrow b\bar{b}$.

3) Chargino diagrams contributing to $Z \rightarrow b\bar{b}$.

4) R_b as a function of top mass for 1) the minimal standard model (MSM), 2) the standard model with a second Higgs doublet (2HD), 3) the minimal supersymmetric standard model (MSSM), assuming $\tan\beta = 1$, $M = 50$ GeV, $\mu = 30$ GeV, $\tilde{m}_t = M_{H^+} = 100$ GeV.

5) $\nabla_b^{(H^+)}$ as a function of M_{H^+}, assuming $m_t = 150$ GeV.

6) Contours for $\nabla_b^{(\chi^+)} \times 100$ as a function of M and μ for $\tan\beta = 1$ and $\tilde{m}_t = 100$ GeV. Lowest dashed lines show limits set from current bounds on chargino masses, as explained in the text. Higher set of dashed lines shows the the corresponding limits which would be set by LEP2. Dotted lines show corresponding limits set by neutralino masses.

7) Contours for $\nabla_b^{(\chi^+)} \times 100$ for $\tan\beta = 10$, $\tilde{m}_t = 100$ GeV.

8) $\nabla_b^{(\chi^+)}$ as a function of $\tilde{m}_t$ for $\tan\beta = 1$ and a) $M, \mu = 50, 30$ GeV, b) $M, \mu = 80, -80$ GeV.

9) Contours for $\nabla_b^{(\chi^+)} \times 100$ as function of mixing angle and heavier squark mass, for $\tan\beta = 1$ and $M, \mu = 50, 30$ GeV.

10) Contours showing chargino contribution to $A_{LR}^b \times 100$, assuming $\tan\beta = 70$ and $\tilde{m}_t = 100$ GeV. The right-handed contribution to $\nabla_b^{(\chi^+)}$ can be obtained by multiplying by -1/2.

11) Neutralino diagrams contributing to $Z \to b\bar{b}$.

12) Contours for $\nabla_b^{(\chi^0)} \times 100$ for $\tan\beta = 70$ and a squark mass of 100 GeV.

13) Contours showing neutralino contribution to $A_{LR}^b \times 100$.

14) Neutral scalar diagrams contributing to $Z \to b\bar{b}$.

15) Contributions to $\nabla_b^{(H)}$ and A_{LR}^b from charged and neutral scalars for $\tan\beta = 70$.

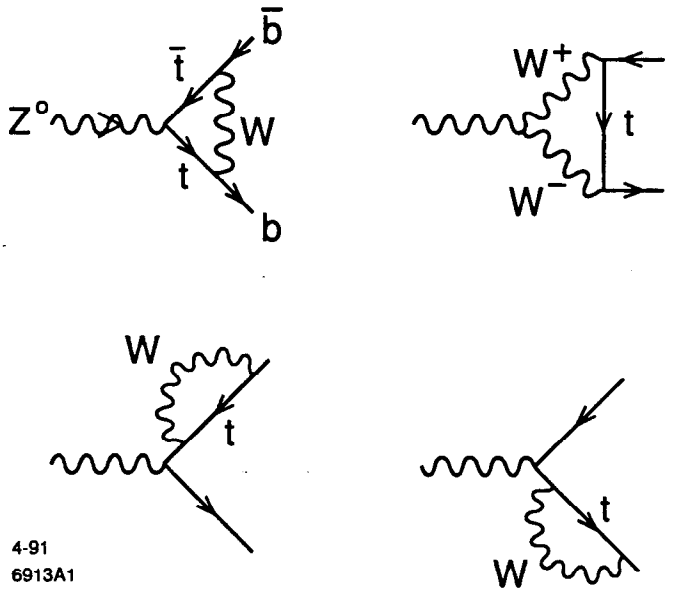

Fig. 1

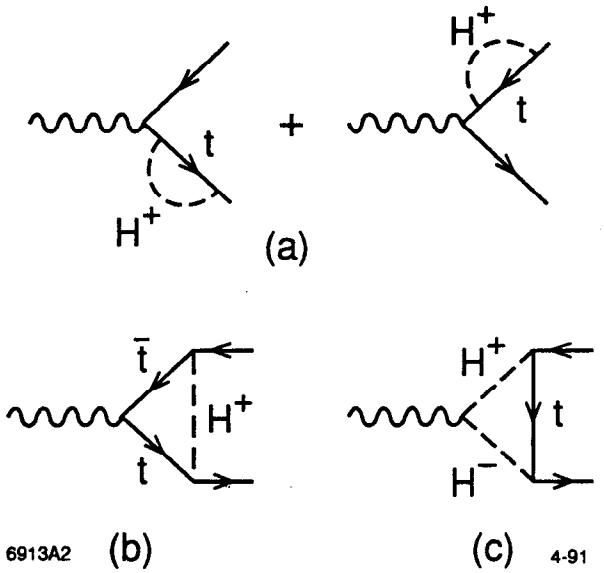

Fig. 2

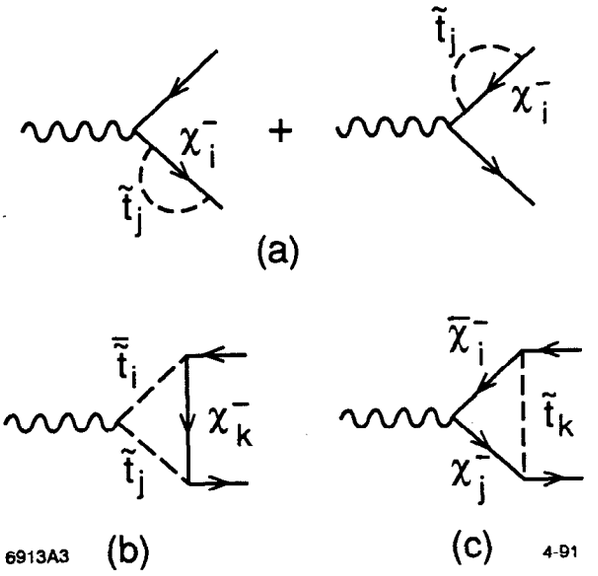
$\tilde{t}_j$
χ_i^-
+
χ_i^-
$\tilde{t}_j$
(a)
$\bar{\tilde{t}}_i$
χ_k^-
$\tilde{t}_j$
$\bar{\chi}_i^-$
$\tilde{t}_k$
χ_j^-
6913A3
(b)
(c)
4-91

Fig. 3

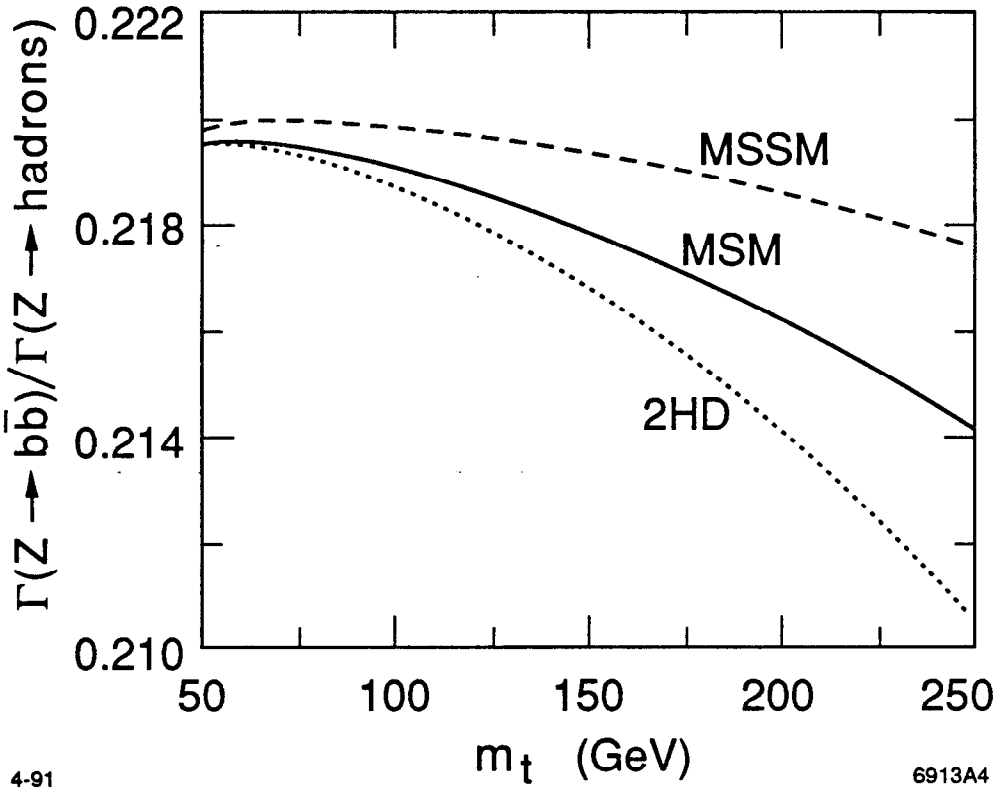
0.222
0.218
0.214
0.210
$\Gamma(Z \to b\bar{b})/\Gamma(Z \to \text{hadrons})$
MSSM
MSM
2HD
50
100
150
200
250
m_t (GeV)
4-91
6913A4

Fig. 4

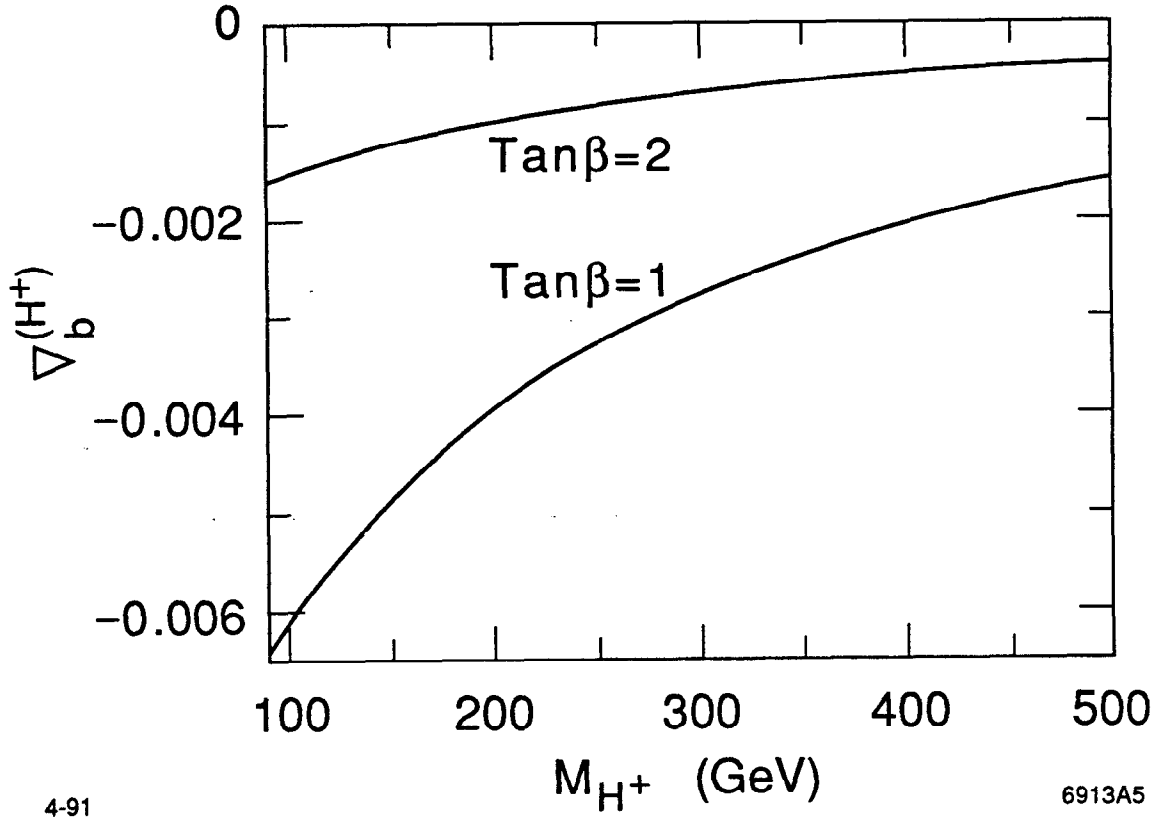
0
-0.002
-0.004
-0.006
Tanβ=2
Tanβ=1
$\Delta_b^{(H^+)}$
100
200
300
400
500
M_{H^+} (GeV)
4-91
6913A5

Fig. 5

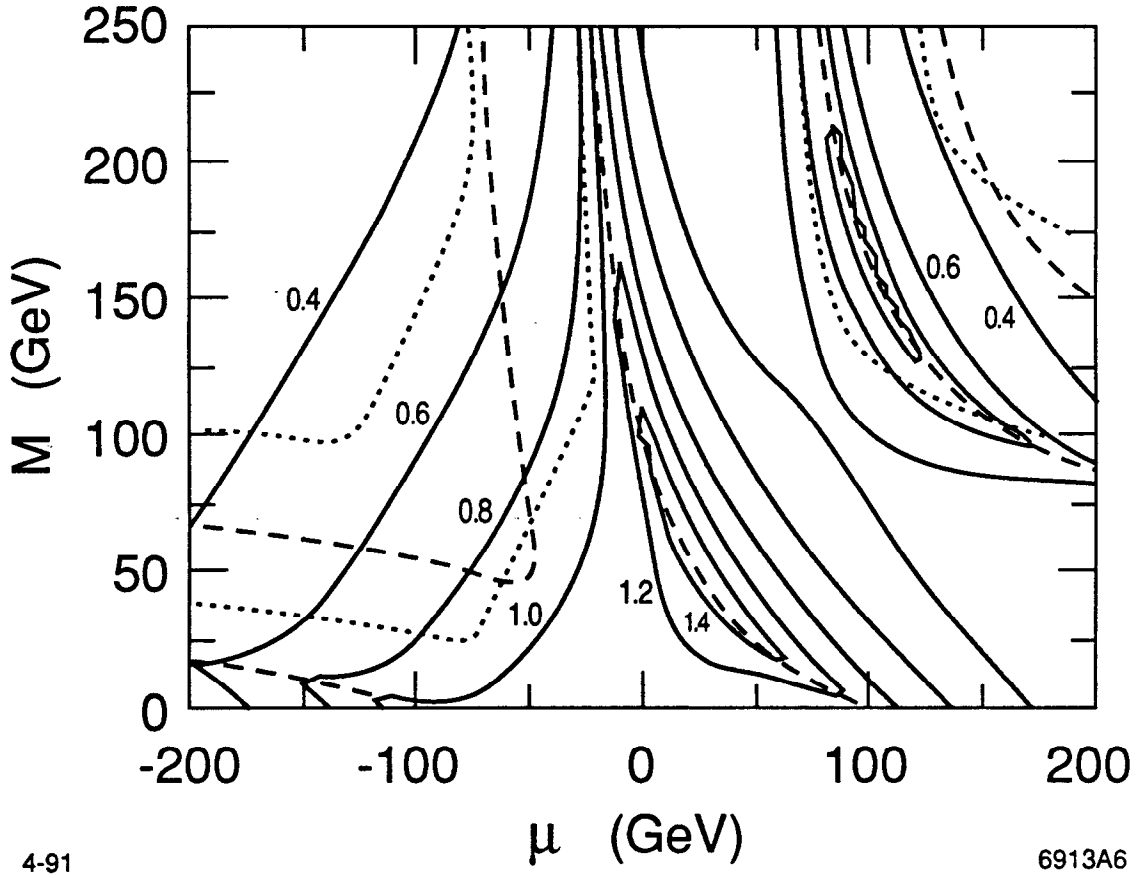
250
200
150
100
50
0
M (GeV)
-200
-100
0
100
200
μ (GeV)
0.4
0.6
0.8
1.0
1.2
1.4
0.6
0.4
4-91
6913A6

Fig. 6

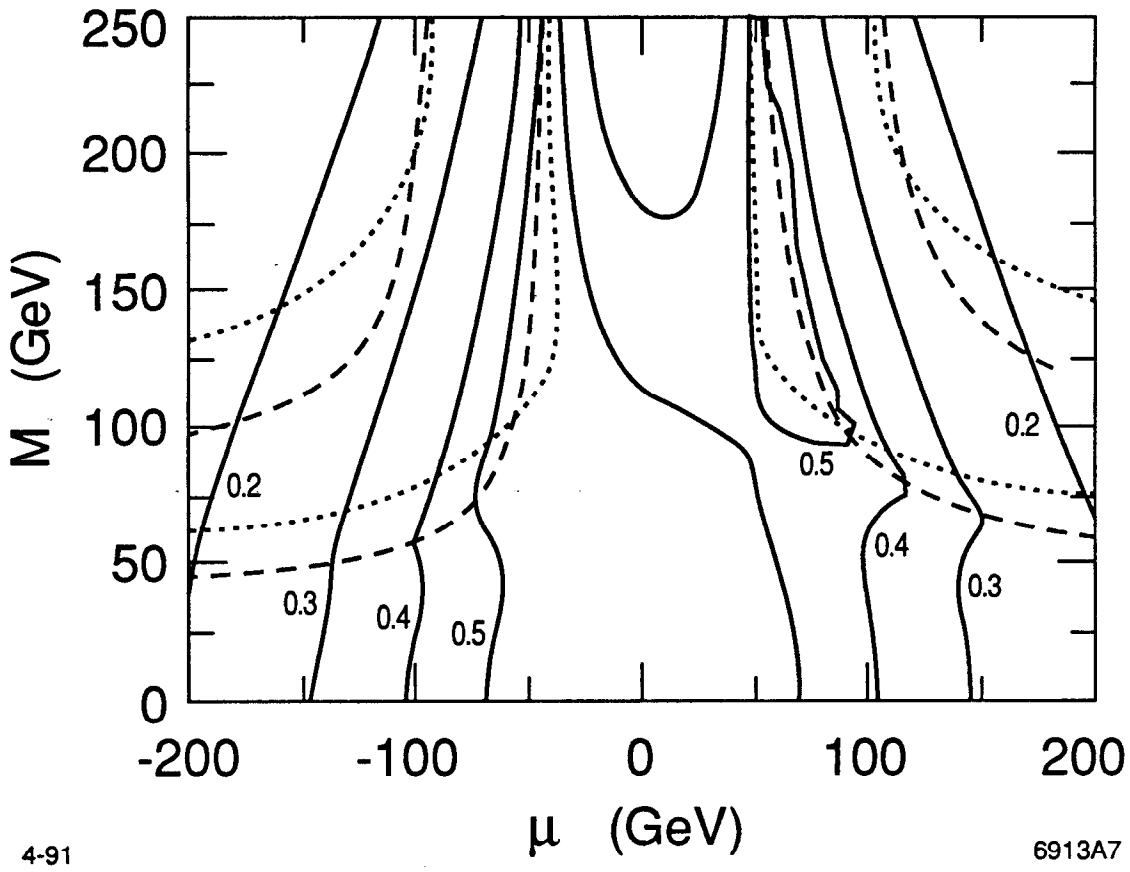
250
200
150
100
50
0
M (GeV)
-200
-100
0
100
200
μ (GeV)
0.2
0.3
0.4
0.5
0.5
0.4
0.3
0.2
4-91
6913A7

Fig. 7

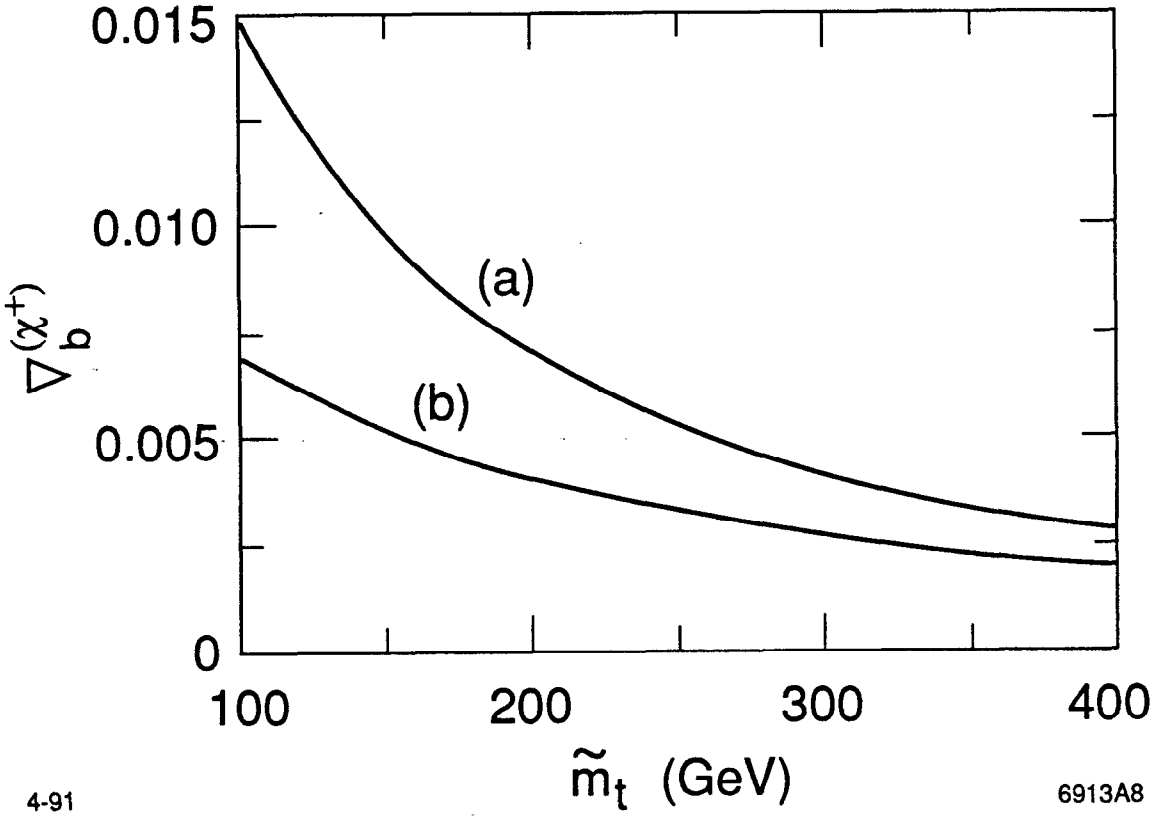
0.015
0.010
0.005
0
100
200
300
400
(a)
(b)
$\nabla_b^{(\chi^+)}$
$\tilde{m}_t$ (GeV)
4-91
6913A8

Fig. 8

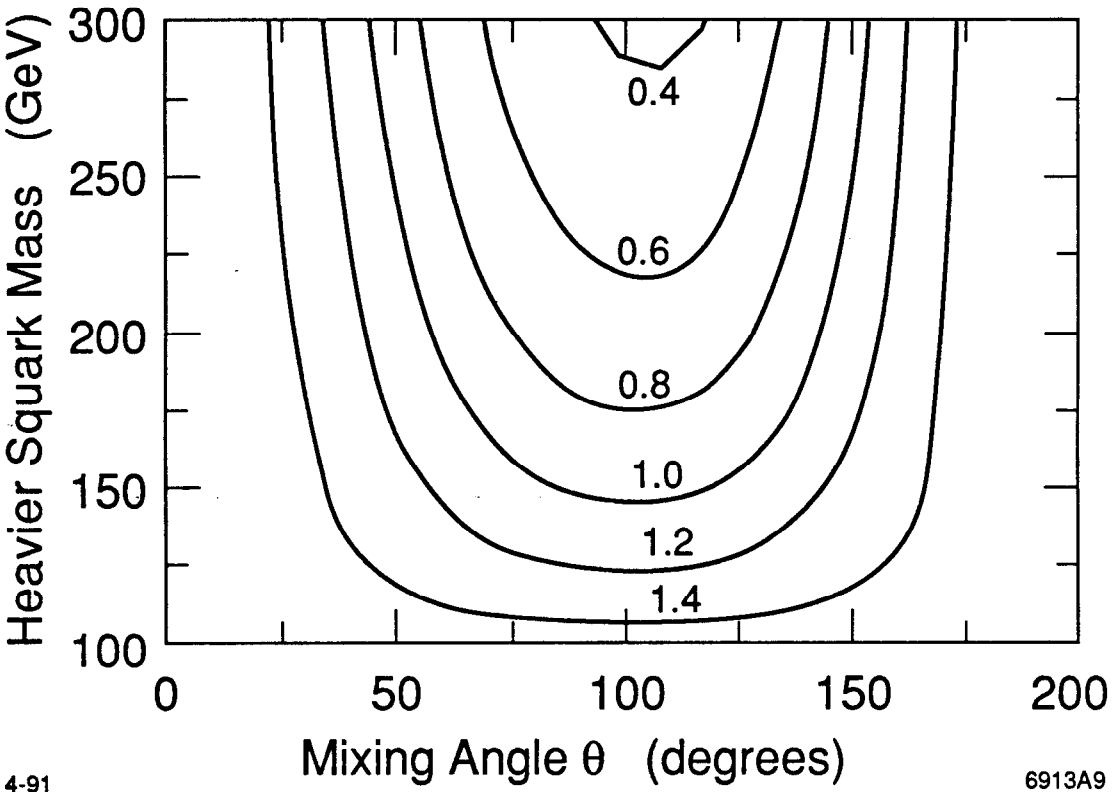
Heavier Squark Mass (GeV)
300
250
200
150
100
0
50
100
150
200
Mixing Angle θ (degrees)
0.4
0.6
0.8
1.0
1.2
1.4
4-91
6913A9

Fig. 9

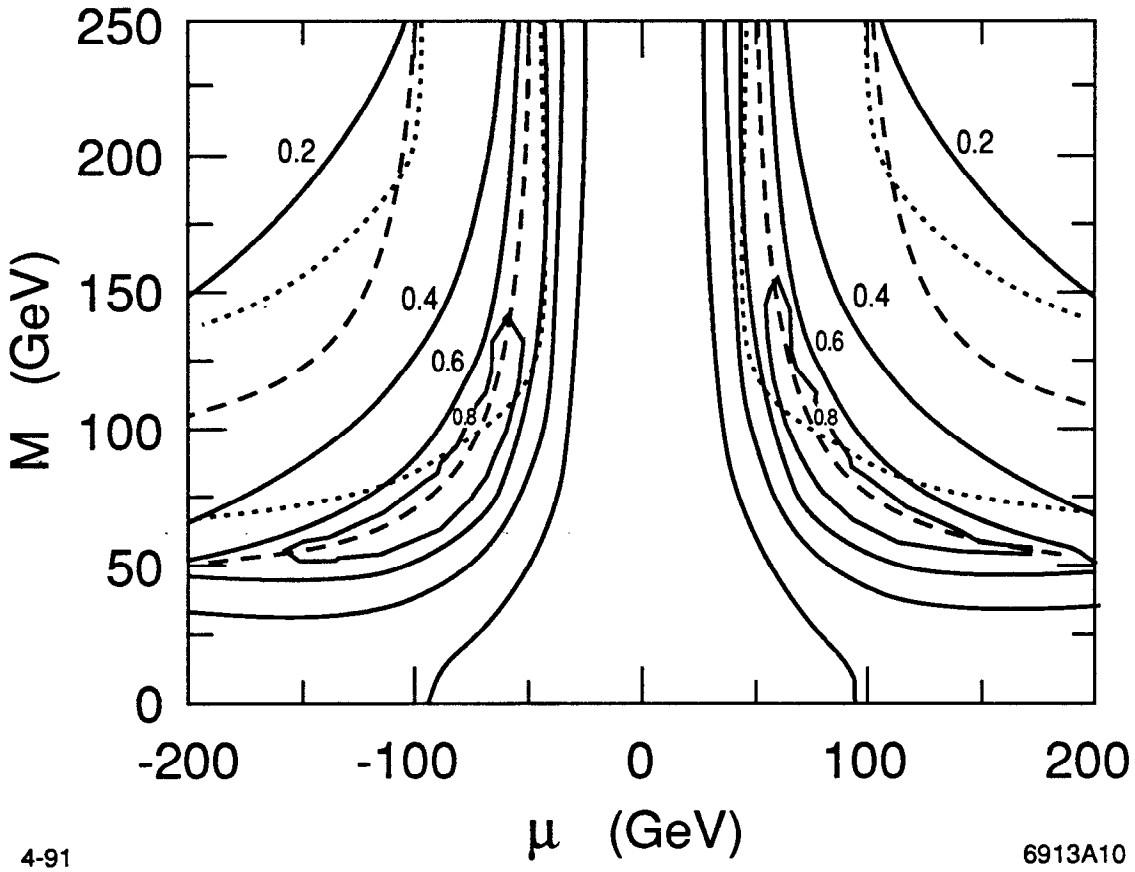
250
200
150
100
50
0
M (GeV)
0.2
0.4
0.6
0.8
0.2
0.4
0.6
0.8
-200
-100
0
100
200
μ (GeV)
4-91
6913A10

Fig. 10

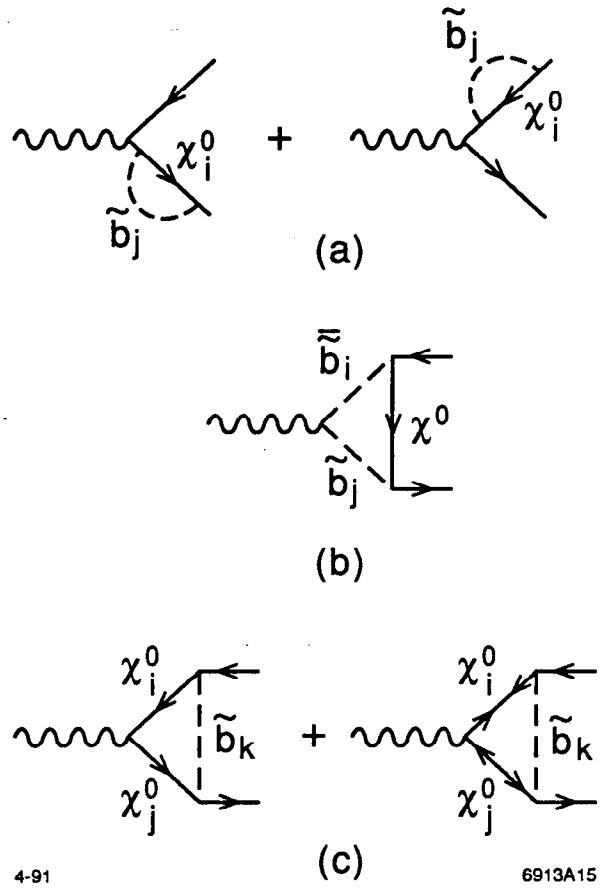
$\tilde{b}_j$
χ_i^0
+
χ_i^0
$\tilde{b}_j$
(a)
$\tilde{\tilde{b}}_i$
χ^0
$\tilde{b}_j$
(b)
χ_i^0
$\tilde{b}_k$
χ_j^0
+
χ_i^0
$\tilde{b}_k$
χ_j^0
(c)
4-91
6913A15

Fig. 11

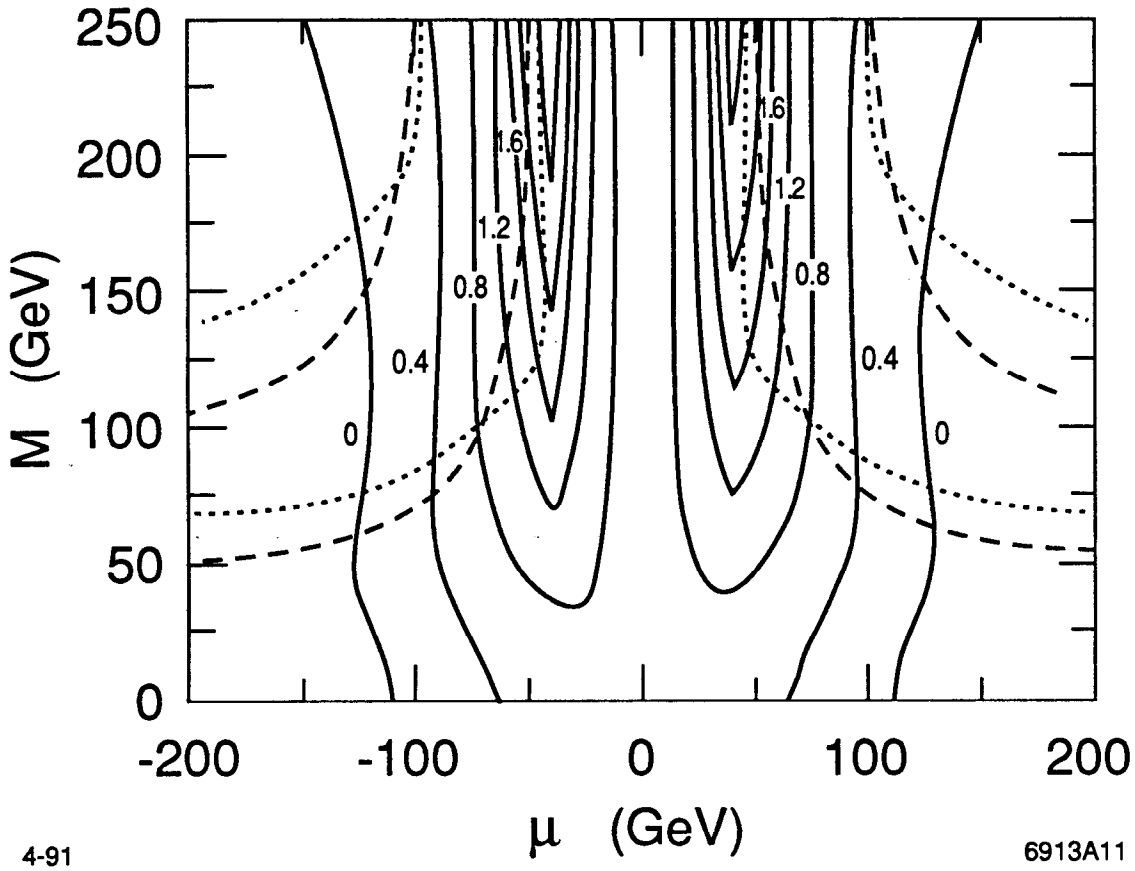
250
200
150
100
50
0
M (GeV)
-200
-100
0
100
200
μ (GeV)
1.6
1.2
0.8
0.4
0
4-91
6913A11

Fig. 12

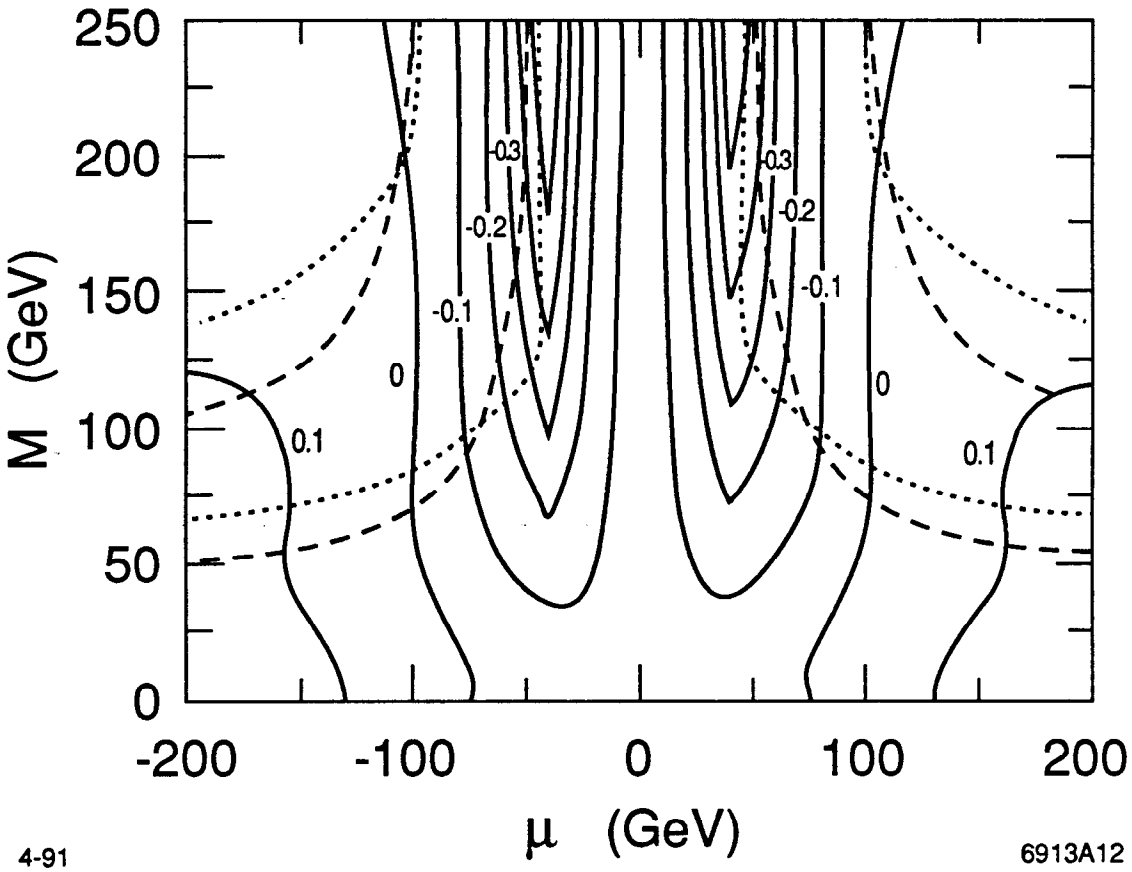

4-91

6913A12

Fig. 13

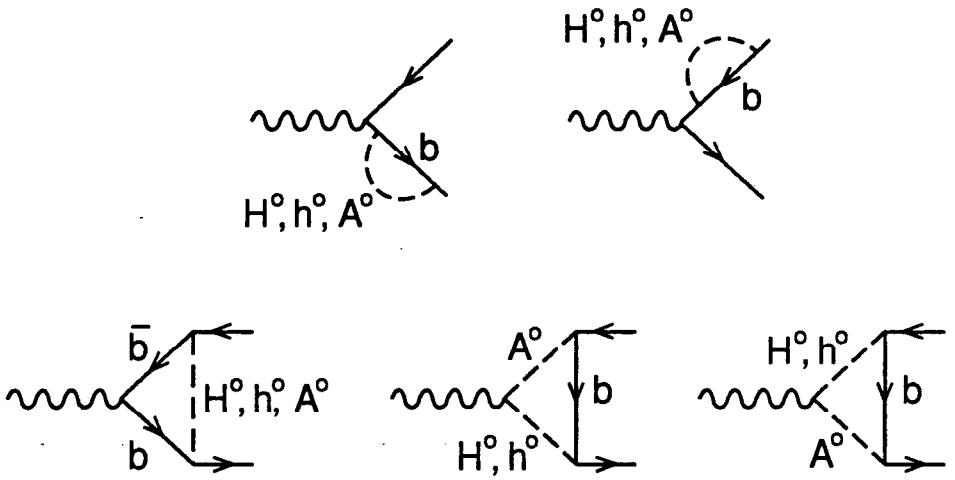

Fig. 14

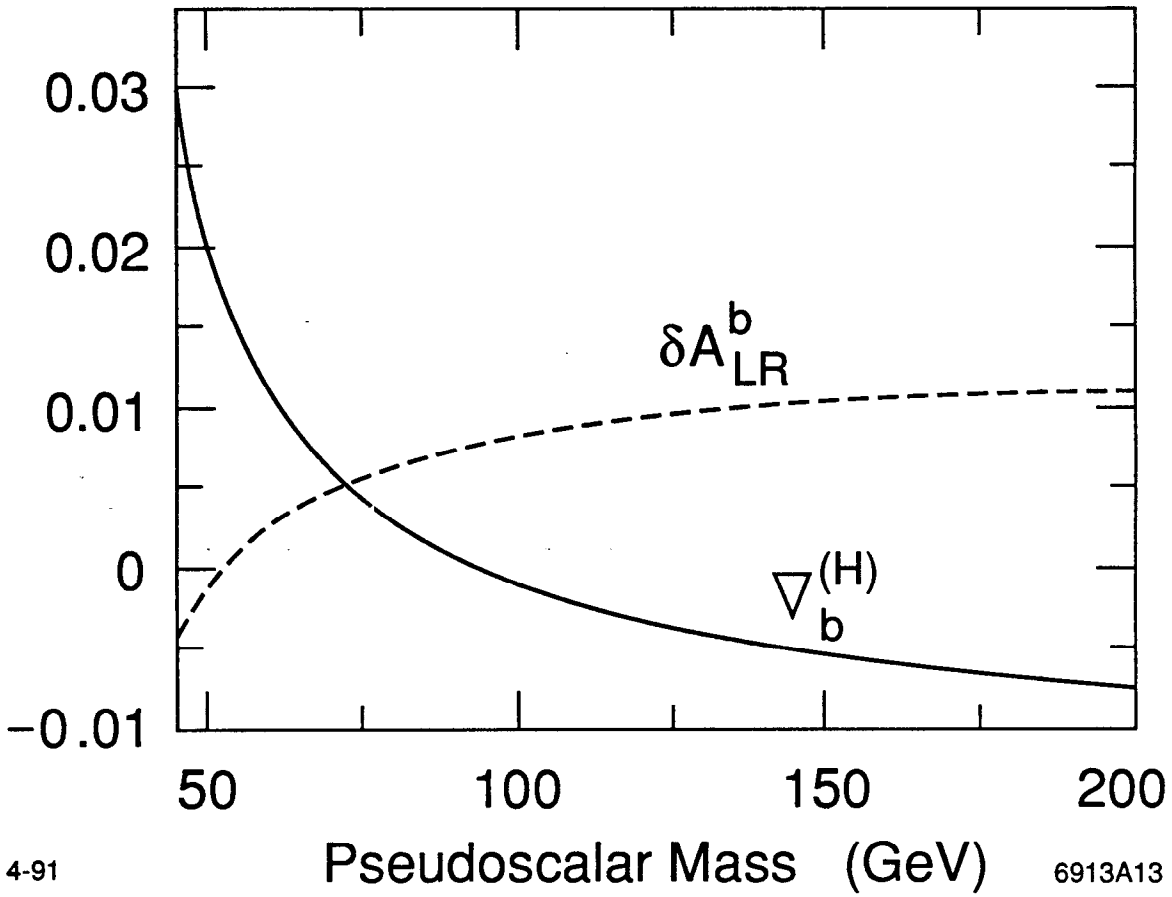
0.03
0.02
0.01
0
-0.01
50
100
150
200
δA_{LR}^{b}
$\nabla_{b}^{(H)}$
Pseudoscalar Mass (GeV)
4-91
6913A13

Fig. 15